ORIGINAL ARTICLE

CrossMark

An adaptive filtering algorithm to estimate sprint velocity using a single inertial sensor

Reed D. Gurchiek[1] · Ryan S. McGinnis[2] · Alan R. Needle[1] · Jeffrey M. McBride[1] · Herman van Werkhoven[1]

Abstract

The assessment of sprint velocity is useful for evaluating performance and guiding training interventions. In this paper, we describe an adaptive filtering algorithm to estimate sprint velocity using a single, sacrum-worn magneto-inertial measurement unit. Estimated instantaneous velocity, average 10 m interval velocity, and peak velocity during 40 m sprints from the proposed method were compared to a reference method using photocell position-time data. Concurrent validity of the proposed method was assessed using mean absolute error and mean absolute percent error for all velocity estimates. The significance of the mean error was assessed using a factorial ANOVA for average interval velocity and a paired-samples t test for peak velocity. Reliability was assessed using Bland–Altman 95% limits of agreement for repeated measures. Average interval velocity was underestimated early in the sprint (-0.25 to -0.05 m/s) and overestimated later (0.13 m/s) with mean absolute error between 0.20 m/s (3.95%) and 0.62 m/s (7.78%). The average mean absolute error was 0.45 m/s (7.02%) for instantaneous velocity and 0.63 m/s (7.84%) for peak velocity. The limits of agreement grew progressively wider at greater distances (-0.59 to 0.34 m/s for 0–10 m and -1.32 to 1.59 m/s for 30–40 m). The estimation error from the proposed method is comparable to other wearable sensor-based methods and suggests its potential use to assess sprint performance.

1 Introduction

An important part of a sprint performance assessment is estimating sprint velocity, which may be used by itself or with other metrics to evaluate performance [1]. Available techniques to assess sprint velocity include the use of photocells

✉ Reed D. Gurchiek
  gurchiekrd@appstate.edu

  Ryan S. McGinnis
  ryan.mcginnis@uvm.edu

  Alan R. Needle
  needlear@appstate.edu

  Jeffrey M. McBride
  mcbridejm@appstate.edu

  Herman van Werkhoven
  vanwerkhovenh@appstate.edu

[1] Appalachian State University, 111 Rivers Street, Boone, NC 28608, USA

[2] University of Vermont, Burlington, USA

[2, 3], lasers [4], radar [3], treadmills [5], global positioning systems (GPS) [6–9], smartphone video [10], and magneto-inertial measurement units (MIMUs) [11, 12]. Of these technologies, the wearable devices (MIMUs and GPS) are advantageous in terms of cost and ease of use. More studies have used GPS than MIMUs to estimate sprint velocity, but these show varying results [6–8] and suggest limited use indoors [13], for short distances [7], and for higher sprint velocities [9].

MIMUs present further advantages for their potential to provide a more comprehensive assessment. Their general use in biomechanics includes estimating joint angles [14], identifying fatigue [15], assessing jumping [16] and change-of-direction [17] performance, and estimating walking [18] and running speed [19]. Specific to sprinting, methods have been developed to identify foot-strike and foot-off events to estimate stance and stride duration [20, 21] and for estimating trunk lean [22] and ground reaction force [23] during the sprint start. Setuain et al. [11] proposed a MIMU-based method to estimate kinetic determinants of sprint performance using velocity and ground reaction force estimates [11]. Their system, however, requires photocell-based position-time data to correct for drift error in the MIMU velocity estimate. Thus, a need still exists for a MIMU-only approach to estimating sprint velocity.

Perhaps the simplest estimation of sprint velocity using MIMU data would be to first estimate the initial orientation of the MIMU in the track frame and then the instantaneous orientation by strapdown integration. Then the MIMU estimate of the acceleration vector could be expressed in the track frame and the forward component time-integrated yielding velocity. This approach would introduce error from various sources (e.g. integration drift [14] or ferromagnetic disturbances [24]), but could be compensated for using measurements from an additional instrument and data fusion techniques [25]. Unless the additional instrument can be incorporated into a wearable device, this addition removes some of the advantages of wearable sensor-based systems. A GPS unit combined with a MIMU on a single sensor could allow error compensation while maintaining these advantages but would limit the system to outdoor use. A single MIMU provides the means to fuse orientation estimates from the on-board accelerometer and/or magnetometer with that obtained using the gyroscope via strapdown integration [14, 26]. Data fusion in this way is only valid when the net acceleration is mostly gravity and when there are no ferromagnetic disturbances. The dynamic nature of sprinting prevents the former and the latter limits the use of magnetometer updates, especially indoors [24]. Thus, the use of some other reference information is needed to provide error compensation, especially as the sprint progresses in time [14].

To the authors' knowledge, the study by [12] is the only one to quantify the error in estimating sprint velocity from only a sacrum-worn MIMU. Their method, however, was based on proprietary algorithms and unspecified constraints. Yang et al. [19] proposed a method incorporating task-constraints for error compensation to estimate constant velocities of relatively low magnitude (≤ 3.5 m/s) and thus it may not be appropriate for sprint running. Similarly, we thought to use characteristics of sprint running as natural constraints to correct MIMU estimates. Namely, we made the following two assumptions about sprint running in a straight line:

I. the heading of a sacrum-worn MIMU during the sprint is expected to be zero-mean
II. the velocity–time relationship is expected to resemble model sprint data.

Regarding assumption (II.), such a model was first proposed by Furusawa et al. [2] describing the motion of a sprinter. The model involves two constants (v_{m} and τ) related to the position (p) at time t by [2, 3],

$$p(t) = v_{\mathrm{m}}\left(t + \tau e^{-\frac{t}{\tau}}\right) - v_{\mathrm{m}}\tau. \tag{1}$$

Then, velocity (v) is given by differentiation,

$$v(t) = v_{\mathrm{m}}\left(1 - e^{-\frac{t}{\tau}}\right). \tag{2}$$

The constants v_{m} and τ in Eq. (2) correspond to, respectively, the horizontal asymptote of the velocity–time curve (velocity one would reach should they sprint indefinitely and never fatigue) and the time it takes to reach 63.21% of v_{m}. Position-time data (from photocells [1, 2] or smartphone video [10]) has been used to estimate v_{m} and τ in Eq. (1) to estimate velocity using Eq. (2).

In this paper, we describe a filtering algorithm incorporating constraints based on assumptions (I) and (II) to estimate sprint velocity from a single MIMU during a 40-m sprint. An experimental protocol was designed to determine the concurrent validity of the proposed method by comparing the velocity estimates to those obtained using photocells.

2 Methods

2.1 Algorithm design

The algorithm developed in this study consists of three basic steps. In the first step, we determine a first estimate of the MIMU orientation during the sprint. In the second step, we employ the orientation correction given by assumption (I.) and in the third step, we employ the velocity correction given by assumption (II.). See Fig. 1 for a summary of the proposed algorithm.

2.1.1 MIMU orientation and vector rotations during the sprint

The quaternion is used to describe the orientation of the sensor frame $\{F_{\mathrm{S}}\}$ relative to the track frame $\{F_{\mathrm{T}}\}$ according to the single rotation through an angle γ about some axis U, of unit length, that would align $\{F_{\mathrm{T}}\}$ with $\{F_{\mathrm{S}}\}$ (Fig. 2) [27]. The instantaneous orientation during the sprint is estimated using a Kalman filter similar to that described in [14] (see Appendix in the Online Supplementary Material for details).
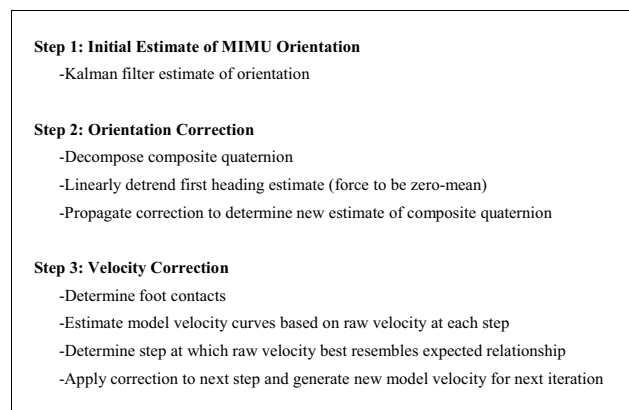
Step 1: Initial Estimate of MIMU Orientation
   -Kalman filter estimate of orientation

Step 2: Orientation Correction
   -Decompose composite quaternion
   -Linearly detrend first heading estimate (force to be zero-mean)
   -Propagate correction to determine new estimate of composite quaternion

Step 3: Velocity Correction
   -Determine foot contacts
   -Estimate model velocity curves based on raw velocity at each step
   -Determine step at which raw velocity best resembles expected relationship
   -Apply correction to next step and generate new model velocity for next iteration
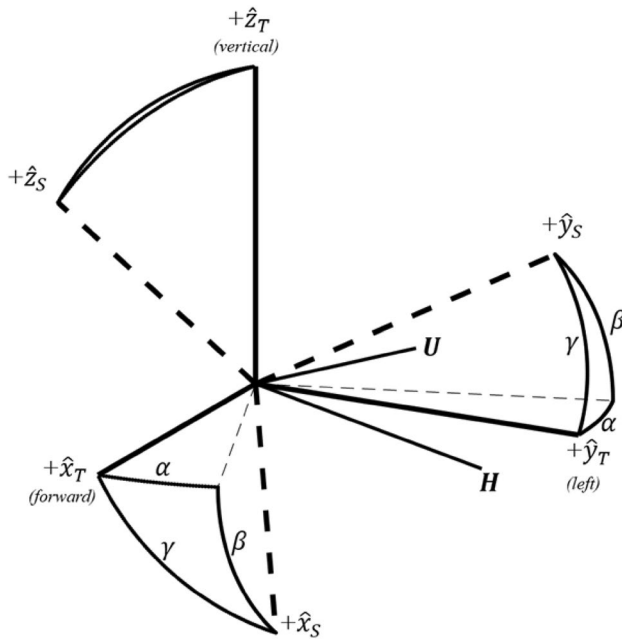
Fig. 1 Description of proposed algorithm

Fig. 2 Description of frame orientations. The track frame axes are the thick solid black lines and the sensor frame axes are the thick dashed black lines. The orientation may be described by a single rotation through an angle γ ($\approx 50°$ in the figure) about the axis labeled U (curved black lines labeled γ) or by two successive rotations: first through an angle α (20° in the figure) about $\hat{z}_T$ (curved black lines labeled α) and then a second rotation through β (45° in the figure) about the axis labeled H (curved black lines labeled β)

The orientation is initialized using sensor referenced measurements of the world frame gravity and local magnetic field vectors [23, 26]. To construct this composite quaternion, we consider two rotations that would align the frames instead of one composite rotation [26, 27]: first about the $\{F_T\}$ vertical axis through an angle α (Q_α), called the sensor's heading, and second about an axis (H) of unit length in the $\{F_T\}$ horizontal plane through an angle $\beta(Q_\beta)$, called the sensor's attitude. First, the accelerometer measurement of the $\{F_T\}$ vertical axis (i.e. the gravity vector) expressed in $\{F_S\}$ determines the MIMU attitude angle β and rotation axis H to estimate Q_β [26]. Second, the magnetometer measurement of the local magnetic field vector expressed in $\{F_S\}$ is rotated to the $\{F_T\}$ horizontal plane using Q_β. The x and y components of the rotated vector determine the MIMU heading angle α to construct Q_α [23]. Then, because Q_α and Q_β are known, Q_γ (the sensor's initial orientation) is given by their quaternion product ($Q_\gamma = Q_\alpha \otimes Q_\beta$) [27]. With this initial orientation, the Kalman filter provides a first estimate of sensor orientation $(Q_\gamma)^-$ throughout the remainder of stance and the sprint.

2.1.2 Filtering algorithm: orientation correction

The second step is to correct the orientation according to assumption (I.): the heading of the runner throughout the entire sprint is expected to be zero-mean. First, Q_γ^- is decomposed into attitude and heading quaternions, Q_β and Q_α^- respectively, and the a priori heading estimate (α^-) extracted. The derivation of the general decomposition is found in [27] (a detailed description is provided in the Appendix in the Online Supplementary Material). We then linearly detrend α^-, enforcing the zero-mean constraint, and use the corrected heading to construct the heading quaternion Q_α to better estimate the composite quaternion (Q_γ). Then, Q_γ is used to rotate the MIMU referenced acceleration vector to $\{F_T\}$ and the forward component is time-integrated to yield an a priori estimate of forward velocity (v^-). The time of the sprint start is defined as the first instant at which v^- exceeds one standard deviation above the average velocity during the interval between the beginning of stance and the first estimate of the sprint start. The latter is a first estimate found by visual inspection of v^- and the former is defined as the end of the 1-s interval of minimal movement (interval during which the sum of the variance of each axis of the accelerometer is a minimum) during the sprint start stance. Similar methods, using a standard deviation threshold measure to detect onset from biological and biomechanical data, have been employed elsewhere (e.g., EMG data [28], acceleration data [29]).

2.1.3 Filtering algorithm: velocity correction

Next, we seek to estimate v_m and τ and the associated model sprint velocity which best characterize the sprint to correct v^- enforcing the constraint allowed by assumption (II.). The only information available to estimate these constants is v^- and while any subset of v^- could be used, the choice may affect the accuracy of the estimates. For example, a larger subset may introduce more drift error, but a smaller subset contains less information to estimate v_m and τ. To solve this problem, we first seek to determine which subset of v^- best resembles the expected relationship in Eq. (2). We consider the subsets of v^- each beginning with the start of the sprint and each ending with a different foot contact (identified using the method described in [21]). The first subset ended with the third foot contact because the first foot contact is not expected to well represent the sprint capabilities throughout the entire sprint [3] and the second may introduce bias in the first model estimate due to bilateral asymmetries. Each subset is low-pass filtered at 1 Hz and fit to Eq. (2) using non-linear least squares curve fitting to determine v_m and τ (Fig. 3). Low-pass filtering at 1 Hz was shown from pilot data to sufficiently remove the sinusoidal nature of sprint velocity not expressed in Eq. (2). Lower and upper bounds were placed on estimates of the constants v_m and τ in Eq. (2) determined using previously published data (three standard deviations above and
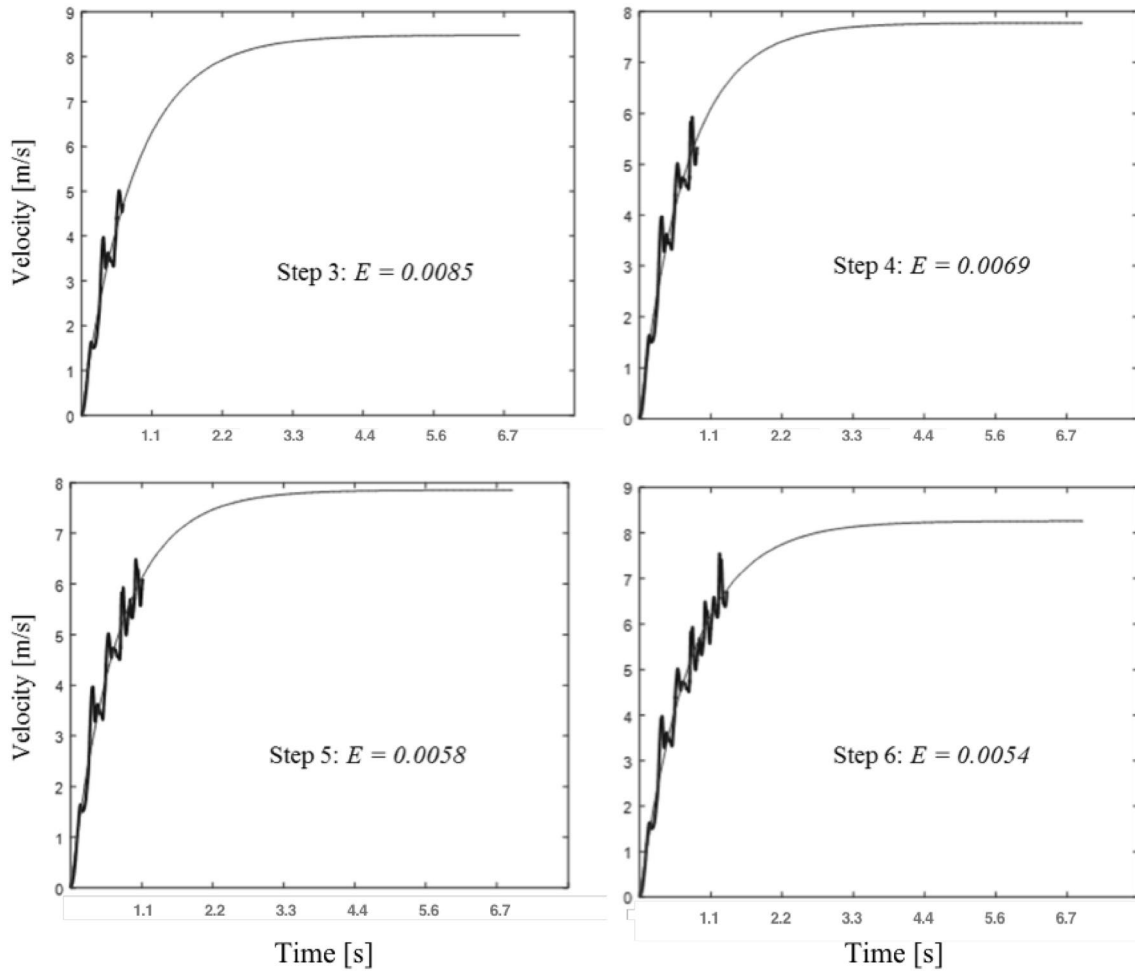
Fig. 3 The a priori velocity (v^-) estimates (thick black line) were used to estimate the model constants v_m and τ in Eq. (2) and the associated model velocity curve (thin gray line) for the subsets of v^- each beginning at the sprint start and ending with a different foot contact

(foot contacts 3 through 6 shown here). The error associated with the curve fitting indicates how well the raw velocity estimate resembled the expected model curve

below the means in [2, 3]). For each subset, the normalized error (E) associated with the curve fitting (squared norm of the residual expressed relative to the number of samples used to generate the curve) indicates how well the data from that subset resembles the expected relationship (see [30] for a similar application) (Fig. 3). Finally, the subset of v^- for which E was a minimum is identified and assumed best representative of the expected model in Eq. (2) (Fig. 4).

The modeled velocity (v_{mod}) based on this subset is then used to provide a correction at the next step, and an iterative correction process for each step is used thereafter. To apply this correction, we find the difference (d_v) between the linear trend of v^- (l_{raw}) and the linear trend of v_{mod} (l_{mod}) from the sample at foot contact $k-1$ (s_{k-1}) to the sample at foot contact $k(s_k)$ according to (Fig. 5),

$$l_{raw} = \frac{v^-_{s_k} - v^-_{s_{k-1}}}{s_k - s_{k-1}}(s) + v^-_{s_{k-1}} \tag{3}$$

$$l_{mod} = \frac{v_{mod,s_k} - v^-_{s_{k-1}}}{s_k - s_{k-1}}(s) + v^-_{s_{k-1}} \tag{4}$$

$$d_v = l_{mod} - l_{raw}, \tag{5}$$

where s is the sample expressed relative to s_{k-1}. The trust given to the correction d_v is dependent on the error associated with v_{mod} generated from the subset ending with foot contact $k-1$ (E_{k-1}) relative to that for foot contact k (E_k). This way the subset more closely resembling the expected relationship in Eq. (2) has a greater contribution to the final estimate. This relative error determines the gain (G) that scales the correction d_v to provide a corrected estimate of the sprint velocity (v) from foot contact $k-1$ to foot contact k according to

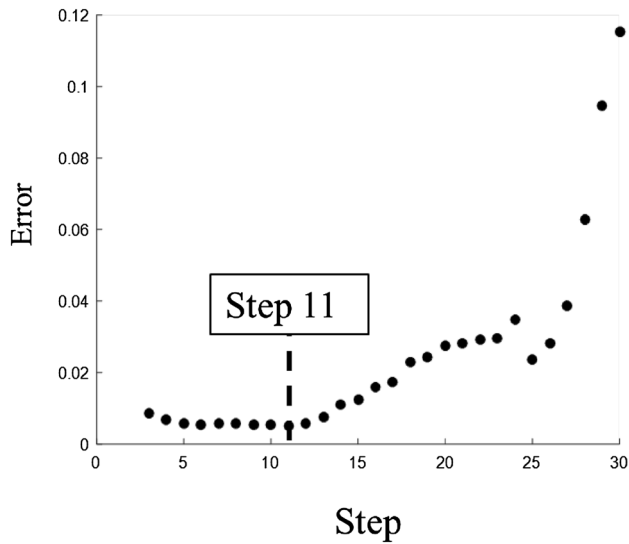$$G = \frac{E_k}{E_k + E_{k-1}} \tag{6}$$

Fig. 4 The error from the curve fitting for each subset of v^- is used to determine which subset best resembles the expected relationship in Eq. (2). Each data point in the figure represents the error associated with the curve fitting of the subset of v^- from the sprint start to step k. The step at which the minimum occurred (step 11 in the figure) represents the subset which best resembles the expected relationship in Eq. (2) and the starting point at which the filter will begin making corrections
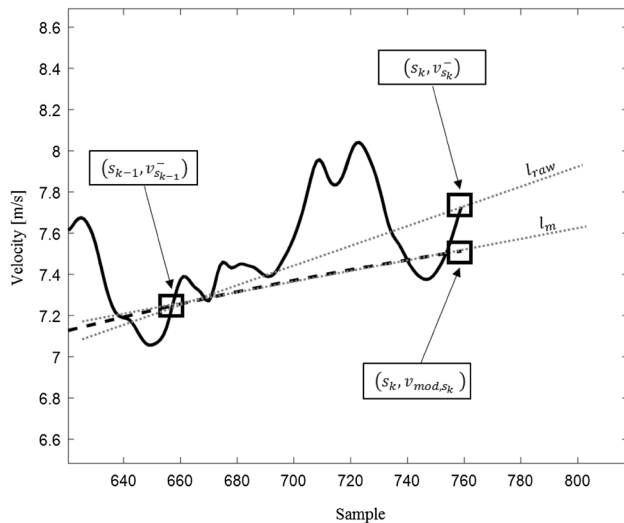

Fig. 5 The difference between the linear trend of the raw velocity estimate (black dotted line labeled l_{raw}) and that of the modeled velocity (gray dotted line labeled l_m) between one foot contact (s_k) and the previous (s_{k-1}) is used to correct the raw velocity estimate. The raw velocity estimate is the solid black line and the modeled velocity is the dashed black line

$$v = v^- + G(d_v). \tag{7}$$

The corrected velocity is used to generate a new model velocity and associated error to be used for the correction at the next foot contact. The position (p) of the sprinter (distance from the start line) is estimated by time-integrating v. We estimate the MIMU initial location behind the start line (p_0) using the trunk lean angle during stance (θ_s), the sprinter's torso length (L_t, distance between the MIMU and the C7 vertebra), and assuming the location of C7 during stance is directly above the start line. The trunk lean angle θ_s is calculated given the MIMU attitude relative to the anatomical frame (β_0) and the MIMU attitude during stance (β_s) by

$$\theta_s = \beta_s - \beta_0 \tag{8}$$

Then p_0 and p are given by

$$p_0 = L_t \sin(\theta_s) \tag{9}$$

$$p = \int_0^{t_k} v \mathrm{d}t - p_0. \tag{10}$$

The corrections continue for each foot contact as long as the condition $p < 40$ m is satisfied.

2.2 Experimental validation

2.2.1 Procedures

An experiment was designed to test the concurrent validity of the proposed method to estimate sprint velocity by comparison to the photocell-based method described by Samozino et al. [3]. To estimate sprint velocity as proposed in [3], five pairs of photocells (Brower Timing Systems, Draper, UT) were positioned along a 40-m straight of an indoor track to collect position-time data at 10 m, 15 m, 20 m, 30 m, and 40 m splits. The timer starts when the sprinter's hand is lifted off a touch sensor. A high-speed video camera (Sensor Technologies America, Carrollton, TX, 200 fps) recorded each subject's sprint start using MaxTRAQ software (Innovision Systems, Columbiaville, MI). The camera was positioned such that the MIMU and hand (on the touch sensor) were within the camera's field of view (Fig. 6). The frames associated with the initial forward movement of the MIMU and of the hand coming off the touch sensor were used to synchronize the two systems.

2.2.2 Subjects

Twenty-eight subjects (12 females, 16 males, age: 20.9 ± 2.3 years, height: 1.73 ± 0.09 m, mass: 71.1 ± 11.7 kg) volunteered to participate in this study. Subjects included collegiate level sprinters and others from the general student population and were included if they were between the ages of 18 and 35 years, reported no musculoskeletal injuries within the 6 months prior to testing, regularly participated
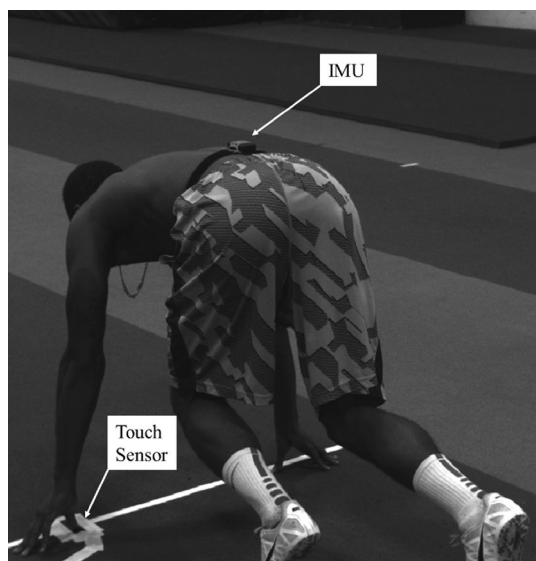
Fig. 6 A high speed video camera was positioned such that the MIMU and the thumb on the touch sensor were visible. The time difference between the lift off of the thumb from the touch sensor and the initial forward movement of the MIMU were used to time-synchronize MIMU and photocell data

in physical activity, and were able to perform maximal effort sprints pain free. All subjects provided written consent to participate. The Appalachian State University Institutional Review Board approved this study.

2.2.3 Inertial measurement units

Yost Data Logger 3-Space Sensors (YEI Technology, Portsmouth, OH) were the MIMUs used in this study. These units have an onboard three-axis accelerometer (range $\pm$ 24 g, noise density: 650 μg/Hz$^{1/2}$, 12-bit resolution), three-axis gyroscope (range $\pm$ 2000°/s, noise density: 0.009°/s/Hz$^{1/2}$, 16-bit resolution), and three-axis magnetometer (range $\pm$ 1.3 Ga, 12-bit resolution). Sampled data from each sensor and the associated timestamp were written to a MicroSD card and downloaded to a computer after data collection for analysis. The sensors were set to sample at 450 Hz; however, the recorded timestamp differences varied (mean 445.72 ± 0.55 Hz). Thus, for all time-integration computations, the recorded time differences were used and not a constant 0.0022 s.

2.2.4 Procedures

Subjects' standing height, mass, and torso length (defined previously) were recorded before undergoing a general and sprint specific warm-up ending with sprint starts from a four-point stance (two hands and two feet). A MIMU was attached to the sacrum using an elastic strap and double-sided tape

(Fig. 6) and a calibration trial was performed while standing straight up with hips aligned with the track. Subjects assumed a four-point stance with one hand on the touch sensor (Fig. 6) and were instructed to be as still as possible. A 3-s countdown was given before the start of a maximal effort 40 m sprint. This sequence was repeated twice more for three total sprints per subject. Three minutes rest was given between sprints or until they felt fully recovered.

2.2.5 Data reduction

All data were processed in MATLAB (MathWorks, Natick, MA). The photocell split-times were fit to Eq. (1) to obtain v_m and τ and used to estimate each subject's instantaneous velocity according to Eq. (2) [3]. MIMU data were used to estimate sprint velocity using the proposed algorithm. Accelerometer and magnetometer data during the standing calibration trial determine β_0 and sensor heading (α_0), respectively [23, 26]. The MIMU initial location is given using β_0 and Eqs. (8) and (9). Because the hips were aligned with $\{F_T\}$ during the calibration trial, α_0 represents the heading of $\{F_T\}$ relative to the local magnetic field vector. Thus, the heading of the MIMU relative to the local magnetic field vector during the sprint stance (α_s) allows an initial estimate of the MIMU heading α relative to $\{F_T\}$,

$$\alpha = \alpha_s - \alpha_0. \tag{11}$$

2.2.6 Statistical analysis

The peak velocity (maximal average velocity between foot contacts), average interval velocity (average velocity over the 0–10 m, 10–20 m, 20–30 m, and 30–40 m intervals), and instantaneous velocity for each sprint was compared between methods. A two-way factorial ANOVA with two within-subjects factors (interval, 4 levels; method, 2 levels) was used to compare the average interval velocities for each 10 m interval. The significance of the differences in peak velocity between the methods was assessed using a paired-samples t test. The error in the MIMU estimates relative to the photocell method was further assessed using mean absolute error (MAE), mean absolute percent error (MAPE), and using Bland–Altman analysis for repeated measures. The latter quantifies the bias (mean error) and 95% limits of agreement (LOA) (compensating for repeated measures within subject) to assess the reliability of the method [31]. Statistical significance for all statistical tests was set a priori at a level of 0.05, with values above this threshold confirmatory of the hypothesis that the estimates obtained between both methods are the same.

3 Results

Ten trials were removed because the 40-m time did not register, leaving 74 available for analysis. The average interval velocities and peak velocity across all subjects determined by the proposed MIMU method and the reference photocell method are shown in Table 1 and the associated error statistics. The factorial ANOVA for the average interval velocity revealed no main effect between methods, ($F_{(1,74)} = 1.667$, $P = 0.201$). A significant interval-by-method interaction effect was observed between distance and method, ($F_{(3,222)} = 17.3$, $P < 0.001$). Pairwise comparisons revealed significant differences between methods for the average velocity estimate during the 0–10 m ($P < 0.001$) and 10–20 m ($P < 0.001$) intervals, but not the 20–30 m ($P = 0.491$) or 30–40 m ($P = 0.128$) intervals. The paired samples t test revealed a significant difference ($P = 0.02$) between the MIMU estimate of peak velocity (8.5 ± 1.24 m/s) and the photocell estimate (8.3 ± 1.09 m/s). The MAE of the MIMU peak and average interval velocity estimates ranged from 0.20 to 0.63 m/s (3.95–7.84%). The Bland–Altman bias (range -0.25 to 0.20 m/s) and LOA (range -0.59 to 0.34 m/s to -1.32 to 1.59 m/s) are given in Table 1 as well as Bland–Altman plots in Figs. 7 and 8. All measurement differences were normally distributed according to the Shapiro–Wilk test and showed no linear trend with the measurement means

Table 1 Error in the estimate of average interval velocities and peak velocity determined by the proposed MIMU method compared to the reference photocell method (all units m/s)

	MIMU mean (SD)	Photocell mean (SD)	MAE (MAPE)	Bias	LOA
Average interval velocity					
0 to −10 m	4.71 (0.41)	4.83 (0.46)	0.20 (3.95%)	−0.12	−0.59, 0.34
10 to −20 m	7.49 (0.86)	7.73 (0.89)	0.42 (5.55%)	−0.25	−1.18, 0.68
20 to −30 m	8.11 (1.09)	8.16 (1.02)	0.50 (6.44%)	−0.05	−1.30, 1.20
30 to −40 m	8.42 (1.24)	8.29 (1.08)	0.62 (7.78%)	0.13	−1.32, 1.59
Peak velocity	8.50 (1.24)	8.30 (1.09)	0.63 (7.84%)	0.20	−1.25, 1.64

MAE mean absolute error, *MAPE* mean absolute percent error, *Bias* mean error, *LOA* Bland–Altman 95% limits of agreement for repeated measures
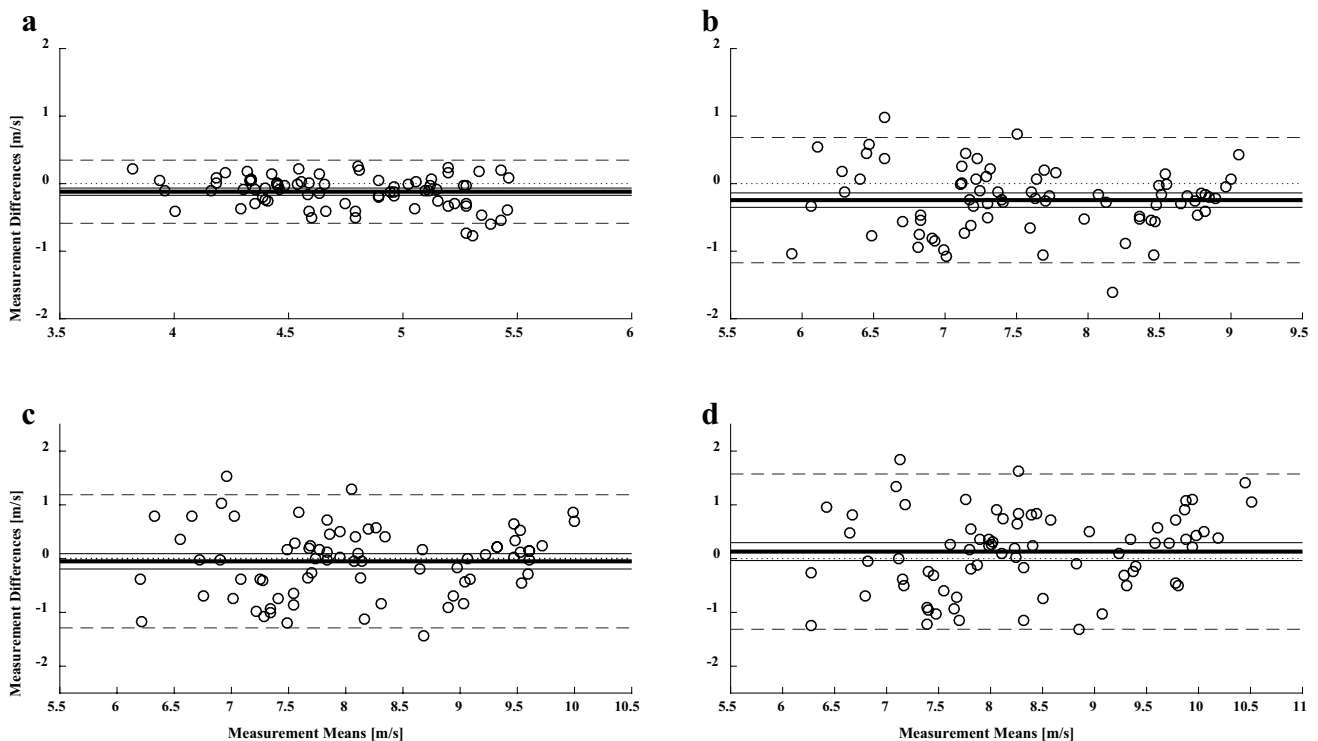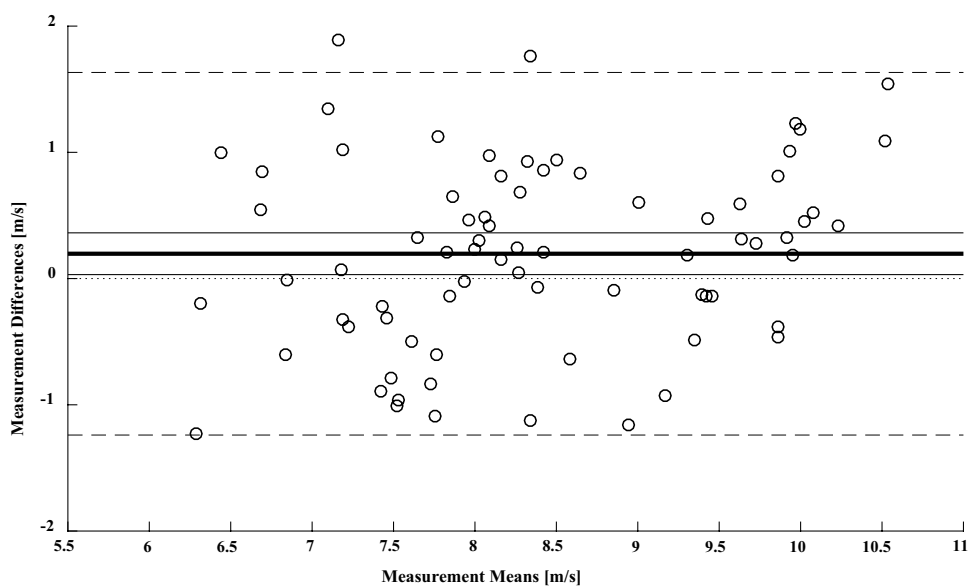

Fig. 7 Bland–Altman plots of average interval velocity. **a** 0–10 m, **b** 10–20 m, **c** 20–30 m, and **d** 30–40 m. Bias: thick solid black line, bias 95% confidence interval: thin solid black line, 95% limits of agreement: dashed black line, line of equality (0): dotted black line

and thus no data were log transformed [32]. The average MAE and MAPE for the instantaneous velocity estimate was 0.45 ± 0.27 m/s and $7.02 \pm 4.02\%$, respectively. Example velocity–time curves comparing the methods are shown in Fig. 9. Figure 10 compares velocity and position versus time data averaged across all subjects between MIMU and photocell methods.

4 Discussion

The Bland–Altman plots show a small bias from the MIMU estimates of velocity (-0.25 to 0.20 m/s) and LOA increasing with sprint velocity. This suggests the velocity estimates from the MIMU method were more consistent early in the sprint compared to later (narrower LOA), but with a slightly greater bias. MAE and MAPE also slightly increased later in the sprint with the greatest error in the peak velocity estimate (MAE $= 0.63$ m/s, MAPE $= 7.84\%$). The factorial ANOVA revealed no systematic differences between the MIMU and photocell estimates of average interval velocity for the final two 10 m splits (Table 1), whereas, despite a lesser MAE, the average interval velocity for the first two 10 m splits was significantly different. This may reflect (1) the MIMU method provides a consistent underestimation early in the sprint, but with greater reliability, (2) the lesser reliability of the MIMU method later in the sprint, and (3) the larger variation in sprint velocity across the subject sample in this study (which becomes more prevalent at greater sprint velocities). The average MAE of the instantaneous sprint velocity (0.45 m/s) is nearly equal to the average MAE across the four average interval velocities (0.44 m/s). This observation further reflects the increasing trend in estimation

error seen in the average interval velocities. Research suggests the actual instantaneous velocity of a sprinter is sinusoidal in nature [5], which agrees with the MIMU estimates (Fig. 9), but is not expressed in the model of Eq. (2). This may explain some of the error in the instantaneous velocity estimate and the reason it was slightly greater than the average MAE of the interval velocities.

The photocell method was the standard of comparison for velocity estimates in this study and thus also for identifying the true constants v_m and τ describing the sprint. Since the proposed method estimates these constants to correct for integration drift, it is informative to compare the constants derived from both methods. The estimate of v_m was not significantly different between methods (MIMU: 8.41 ± 1.32 m/s, photocell: 8.36 ± 1.13 m/s, $p = 0.61$), but the MIMU estimate of τ (1.11 ± 0.20 s) was significantly greater ($p < 0.01$) than the photocell estimate (1.00 ± 0.17 s). Analytically, a larger τ results in a delayed progression to v_m in Eq. (2). Thus, the overestimate of τ from the proposed method may underlie the underestimate of velocity observed early in the sprint (Fig. 10). It may seem contradictory that the MIMU estimate of average v_m was less than the average peak velocity, but this may reflect inaccurate foot contact estimates and/or characteristics of the true sprint velocity not expressed in Eq. (2) (e.g. a sinusoidal nature and bilateral asymmetries).

Although the algorithm used in [12] to estimate sprint velocity is not given in detail, it is the only other study to compare our results to for MIMU-only methods. Thus, we performed post hoc analyses to determine Pearson's correlation coefficients between the MIMU and photocell-determined estimates of velocity. Results between studies show similar bias for peak velocity, MAPE $< 10\%$, and strong relationships ($r \geq 0.75$) between MIMU estimates and

Fig. 9 Comparing raw velocity obtained from direct integration (solid gray line), filtered velocity from the proposed algorithm (solid black line), and model velocity obtained from the reference photocell method (dashed black line). Each curve represents a single subject. **a** An example where direct integration overestimated the true velocity and **b** an example where direct integration underestimated the true velocity
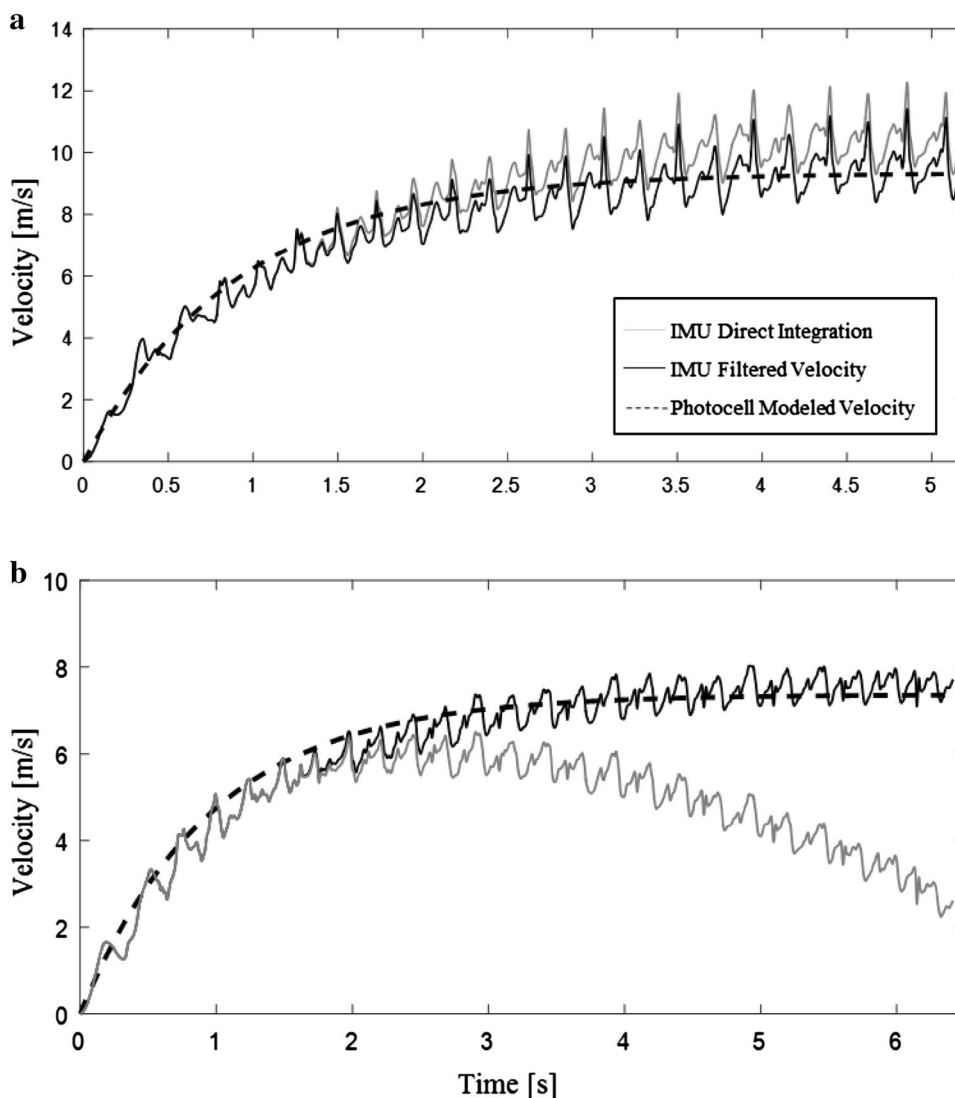
reference measurements for both average interval and peak velocity (except for the 0–10 m average interval velocity in [12] where $r = 0.32$). We also compared our results to that obtained using wearable GPS units as presented in [6] and found comparable reliability and less overall error for the MIMU method in estimating both velocity and distance (distance error at 30 m: GPS $= -2.02$ m, MIMU $= -0.77$ m).

4.1 Limitations

The results of this study only apply to maximal effort 40 m sprints in a straight line undertaken in a non-fatigued state. The initial heading estimates are based on an assumed negligible difference between the local magnetic field vector at the location of the sensor during the standing calibration trial and during the sprint start stance. Ferromagnetic disturbances may invalidate these assumptions and indeed we found an average difference in the magnetic field magnitude between these two locations (0.06 Gauss, 7.18%) which may have introduced an initial heading error. However, the correction in the proposed algorithm forcing the heading-time series during the sprint to be zero-mean also adjusts the initial heading and thus may compensate for this potential error. Finally, the proposed method is not fully automated and does require minimal user input to identify the static intervals prior to the sprint.

5 Conclusion

The low MAE, low MAPE, and low bias between velocity estimates from the proposed MIMU method and reference photocell measurements support the potential use of

Fig. 10 The average model velocity (**a**) generated from the MIMU method (dashed black line) was compared to the reference photocell method (solid black line) as well as the corresponding sprint distance (**b**). The dotted and dashed-dotted lines show the standard deviations of the photocell and MIMU method sprint data respectively. The proposed MIMU method accurately estimated the constant, v_{m}, but significantly overestimated the time constant τ resulting in a slight overestimation of t_{40} for the MIMU method (average t_{40} photocell: 5.87 s, average t_{40} MIMU: 5.91 s)
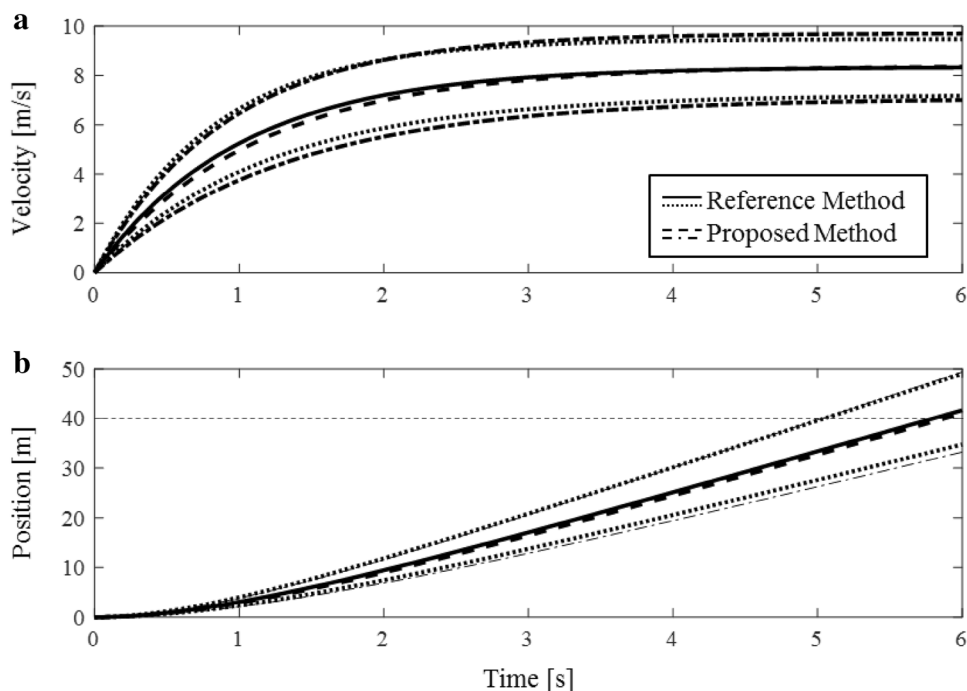
MIMUs for evaluating sprint performance. The estimation error of velocity and reliability of the method are comparable to that reported for other wearable sensor-based methods [6, 12]. The proposed method should only be used for maximal effort, 40-m, straight line sprints when the sprinter is fully recovered until the method is validated for use in other applications.

References

1. Rabita G et al (2015) Sprint mechanics in world-class athletes: a new insight into the limits of human locomotion: sprint mechanics in elite athletes. Scand J Med Sci Sports 25(5):583–594
2. Furusawa K, Hill AV, Parkinson JL (1927) The dynamics of 'sprint' running. Proc R Soc Lond Ser B Contain Pap Biol Character 102(713):29–42
3. Samozino P et al (2016) A simple method for measuring power, force, velocity properties, and mechanical effectiveness in sprint running: simple method to compute sprint mechanics. Scand J Med Sci Sports 26(6):648–658
4. Bezodis NE, Salo AIT, Trewartha G (2012) Measurement error in estimates of sprint velocity from a laser displacement measurement device. Int J Sports Med 33(6):439–444
5. Morin JB, Samozino P, Bonnefoy R, Edouard P, Belli A (2010) Direct measurement of power during one single sprint on treadmill. J Biomech 43(10):1970–1975
6. Waldron M, Worsfold P, Twist C, Lamb K (2011) Concurrent validity and test–retest reliability of a global positioning system (GPS) and timing gates to assess sprint performance variables. J Sports Sci 29(15):1613–1619
7. Petersen C, Pyne D, Portus M, Dawson B (2009) Validity and reliability of GPS units to monitor cricket-specific movement patterns. Int J Sports Physiol Perform 4(3):381–393
8. Varley MC, Fairweather IH, Aughey RJ (Jan. 2012) Validity and reliability of GPS for measuring instantaneous velocity during acceleration, deceleration, and constant motion. J Sports Sci 30(2):121–127
9. Jennings D, Cormack S, Coutts AJ, Boyd L, Aughey RJ (2010) The validity and reliability of GPS units for measuring distance in team sport specific running patterns. Int J Sports Physiol Perform 5(3):328–341
10. Romero-Franco N et al (2016) Sprint performance and mechanical outputs computed with an iPhone app: comparison with existing reference methods. Eur J Sport Sci 17:1–7
11. Setuain I, Lecumberri P, Ahtiainen JP, Mero AA, Häkkinen K, Izquierdo M (2018) Sprint mechanics evaluation using inertial sensor-based technology: a laboratory validation study. Scand J Med Sci Sports 28(2):463–472
12. Parrington L, Phillips E, Wong A, Finch M, Wain E, MacMahon C (2016) Validation of inertial measurement units for tracking 100 m sprint data. In: 34th Int. conf. biomech. sport
13. Seco-Granados G, Lopez-Salcedo J, Jimenez-Banos D, Lopez-Risueno G (2012) Challenges in indoor global navigation satellite systems: unveiling its core features in signal processing. IEEE Signal Process Mag 29(2):108–131
14. Sabatini AM (2011) Estimating three-dimensional orientation of human body parts by inertial/magnetic sensing. Sensors 11(12):1489–1525
15. Lidstone DE, Stewart JA, Gurchiek R, Needle AR, van Werkhoven H, McBride JM (2017) Physiological and biomechanical responses to prolonged heavy load carriage during level treadmill walking in females. J Appl Biomech 33(4):248–255
16. McGinnis RS, Cain SM, Davidson SP, Vitali RV, Perkins NC, McLean SG (2016) Quantifying the effects of load carriage and fatigue under load on sacral kinematics during countermovement vertical jump with IMU-based method. Sports Eng 19(1):21–34

17. McGinnis RS, Cain SM, Davidson SP, Vitali RV, McLean SG, Perkins NC (2015) Inertial sensor and cluster analysis for discriminating agility run technique. IFAC Pap 48(20):423–428

18. McGinnis RS et al (2017) A machine learning approach for gait speed estimation using skin-mounted wearable sensors: from healthy controls to individuals with multiple sclerosis. PLoS One 12(6):e0178366

19. Yang S, Mohr C, Li Q (2011) Ambulatory running speed estimation using an inertial sensor. Gait Posture 34(4):462–466

20. Bergamini E, Picerno P, Pillet H, Natta F, Thoreux P, Camomilla V (2012) Estimation of temporal parameters during sprint running using a trunk-mounted inertial measurement unit. J Biomech 45(6):1123–1126

21. Wixted AJ, Billing DC, James DA (2010) Validation of trunk mounted inertial sensors for analysing running biomechanics under field conditions, using synchronously collected foot contact data. Sports Eng 12(4):207–212

22. Bergamini E, Guillon P, Camomilla V, Pillet H, Skalli W, Cappozzo A (2013) Trunk inclination estimate during the sprint start using an inertial measurement unit: a validation study. J Appl Biomech 29(5):622–627

23. Gurchiek RD, McGinnis RS, Needle AR, McBride JM, van Werkhoven H (2017) The use of a single inertial sensor to estimate 3-dimensional ground reaction force during accelerative running tasks. J Biomech 61:263–268

24. de Vries WHK, Veeger HEJ, Baten CTM, van der Helm FCT (2009) Magnetic distortion in motion labs, implications for validating inertial magnetic sensors. Gait Posture 29(4):535–541

25. Simon D (2006) Optimal state estimation. Wiley, Hoboken

26. Favre J, Jolles BM, Siegrist O, Aminian K (2006) Quaternion-based fusion of gyroscopes and accelerometers to improve 3D angle measurement. Electron Lett 42(11):612–614

27. Kuipers JB (1999) Quaternions and rotation sequences. Princeton University Press, Princeton

28. Hodges PW, Bui BH (1996) A comparison of computer-based methods for the determination of onset of muscle contraction using electromyography. Electroencephalogr Clin Neurophysiol 101(6):511–519

29. Martinez-Mendez R, Sekine M, Tamura T (2011) Detection of anticipatory postural adjustments prior to gait initiation using inertial wearable sensors. J Neuroeng Rehabil 8:17

30. Nichols JA, Bednar MS, Havey RM, Murray WM (2016) Decoupling the wrist: a cadaveric experiment examining wrist kinematics following midcarpal fusion and scaphoid excision. J Appl Biomech 33:1–29

31. Atkinson G, Nevill AM (1998) Statistical methods for assessing measurement error (reliability) in variables relevant to sports medicine. Sports Med 26(4):217–238

32. Giavarina D (2015) Understanding Bland–Altman analysis. Biochem Med 25(2):141–151